All-optical tunable plasmonic nano-aggregations for surface-enhanced Raman scattering

Article *in* Nanoscale · June 2019

DOI: 10.1039/C9NR04906A

Nanoscale

PAPER

View Article Online
View Journal | View Issue

Cite this: *Nanoscale*, 2019, **11**, 13558

All-optical tunable plasmonic nano-aggregations for surface-enhanced Raman scattering†

Lei Chen,[a] Wei Liu,[a] Dongyi Shen,[a] Yuehan Liu,[b] Zhihao Zhou,[b] Xiaogan Liang[c] and Wenjie Wan*[a,b]

Received 10th June 2019,
Accepted 26th June 2019

DOI: 10.1039/c9nr04906a

rsc.li/nanoscale

Interparticle forces play a crucial role in nanoparticle-based nanoscience and nanoengineering for synthesizing new materials, manipulating nanoscale structures, understanding biological processes and ultrasensitive sensing. Complicated by the fluid-dynamical and chemical nature of the liquid environment of nanoparticles, previous attempts are limited to electromagnetic and chemical methods. Alternatively, optically induced forces provide a convenient and fabrication-free route to manipulate nanoparticles at the nanoscale. Here we demonstrate a new double laser trapping scheme for metallic nano-aggregation by inducing strong near-field optical interparticle forces without any chemical agents or complicated fabrication processes. These induced optical forces arising from strong localized plasmon resonance strongly depend on the interparticle separation well beyond the diffraction limit and the polarization of the incident laser field. We examine such sub-resolved interparticle separation in trapped nanoaggregates by measuring surface-enhanced Raman scattering, and further demonstrate the single-molecule sensitivity by implementing such nanostructures. This new technique opens a new avenue for all-optical manipulation of nanomaterials as well as ultra-sensitive bio-chemical sensing applications.

1. Introduction

Metallic nanostructures with nanometer-scale gaps have recently received considerable research interest for strongly enhancing capacitive electromagnetic and optical interactions due to nano-size gap spacing. These nanostructures, often featured with near-field hot spots in their nano-gaps, make them promising platforms for important applications like surface-enhanced Raman scattering (SERS),[1,2] sensitive biosensing,[3,4] surface-enhanced photoemission,[5,6] and enhanced nonlinear optical processes.[7,8] Here the gap spacing inside metallic nanostructures plays a crucial role in field enhancement down to the nanometer scale,[9–12] which requires highly demanding fabrications and this halts their applications. So far, most of such composite nanostructures are permanently fixed structures, fabricated *via* either nanofabrication or self-assembly of colloidal metal nanoparticles.[13,14] However, these methods are either complicated and expensive or time-consuming, or lack tunability of the gap size at small scales. Alternatively, controlled aggregation of colloidal metal nanoparticles[15–19] offers a convenient and less-demanding fabrication method for the same purpose in solution. But how to realize the dynamic assembly of plasmonic nanoparticles with controllable nanometer gaps in these nanostructures, especially in a fluid medium, becomes a key problem. Control of the interparticle distance involves many challenges such as controlling the surface potential and thermal fluctuations of metal nanoparticles, well-characterized by the theory of Derjaguin–Landau–Verwey–Overbeek (DLVO),[15,20] which states that the interparticle interaction in colloids is dominated by additive forces due to screened electrostatic repulsion and van der Waals attraction. Previously, the most common aggregation method for SERS studies is the addition of sodium chloride or pyridine to silver or gold nanoparticles stabilized by negatively charged citrate ions. Sodium chloride induces aggregation by screening surface charges, while neutral pyridine displaces the charged citrate and decreases particle–particle repulsion. These chemicals agglomerate the nanoparticles irreversibly, and hence the aggregates cannot be further used as uniformly dispersed, plasmonic nanoscale entities. Also, such a procedure of aggregation is not conducive for micro/nano-fluidic environments, where a relatively small aggregate can block the

[a]*The State Key Laboratory of Advanced Optical Communication Systems and Networks Department of Physics and Astronomy, Shanghai Jiao Tong University, Shanghai 200240, China. E-mail: wenjie.wan@sjtu.edu.cn*
[b]*MOE Key Laboratory for Laser Plasmas and Collaborative Innovation Center of IFSA, the University of Michigan-Shanghai Jiao Tong University Joint Institute, Shanghai Jiao Tong University, Shanghai 200240, China*
[c]*Department of Mechanical Engineering, University of Michigan, Ann Arbor, MI 48109, USA*

†Electronic supplementary information (ESI) available. See DOI: 10.1039/c9nr04906a

flow of the liquid. Therefore, there is an imperative need to temporarily assemble nanoparticles in a controlled way, and redisperse them back in the fluid after SERS interrogation.

Alternatively, optical forces are well-known in the field of laser tweezers, developed by Ashkin and co-workers in the 80s,[21] as a method to trap, sort and manipulate nano/micro-particles using a tightly focused laser beam, as recently demonstrated by the trapping of silver[22] and gold colloids.[23] However, interparticle optical forces have received less attention until recently. It becomes an evitable and emerging problem beyond one-particle limit for optical trapping in the colloid system.[24–26] These light induced interparticle forces can occur over a range of length scales: in the far-field limit, *i.e.*, $d \gg \lambda$, the light can induce binding force for microscopic size particles.[27] Optical forces arising from the application of optical-frequency electromagnetic fields provide a tunable, chemical-free way to organize metallic nanoparticles in the colloid.[27] In the near-field, *i.e.*, $d \ll \lambda$, the optical fields between adjacent metallic particles are strongly enhanced to create hot-spots, which generate a huge gradient attractive force given the nanometer spatial sizes, better than most lens-based optical trapping techniques.[24,26,28] The interparticle forces arise even if the incident field has no potential gradient; in this sense, the particles self-direct their own assembly.[24,29,30] As a result, optically induced nanoclusters and nanoaggregates can be observed due to these strong interparticle forces.[28] Meanwhile, these strong local enhanced fields can be subsequently applied to SERS applications.[31] However, up to now, salt still needs to be added to the colloidal solution to promote aggregation,[15,17,19,20] which, as stated above, may be harmful for some chemical-sensitive applications. Therefore, achieving all-optically tunable interparticle forces for metallic colloid systems is in high demand.

In this letter, we demonstrate all-optical tunable metallic nano-aggregations based on a double-laser trap to induce strong near-field optical interparticle forces. Unlike previous studies, average interparticle spacing among the nanoparticles purely depends on trapping lasers' power reducing the need for addition chemical agents. These induced optical forces arising from strong localized plasmon resonance strongly affect the interparticle separation deep below the optical diffraction limit, which also posed a great challenge previously for such nano-structure characterization. Alternatively, we examine such sub-resolved interparticle separation in trapped nano-aggregates by measuring surface-enhanced Raman scattering (SERS). Furthermore, we successfully demonstrate the single-molecule sensitivity capability by implementing such nano-structures for SERS applications. This new technique enables new possibilities for all-optical manipulation of nano-materials as well as ultra-sensitive bio-chemical sensing applications.

2. Results and discussion

2.1 Double laser trapped nano-aggregations

Our all optically controllable nano-aggregations are achieved in a double trap experimental scheme as shown in Fig. 1. The first laser trap from a 1064 nm near-infrared (NIR) continuous-wave of a fiber laser (NKT Photonics, Koheras BoostiK Y10) acts as a "macroscopic" trap to confine GNPs in its focus region and encourages interparticle interactions for secondary trapping, where a 532 nm green laser is used to induce such interparticle interactions when the particles are in close proximity. Meanwhile, such a green laser can also serve as the pump source to excite SERS, which will be elaborated later. Note that, a sole green laser cannot form a stable optical trap,

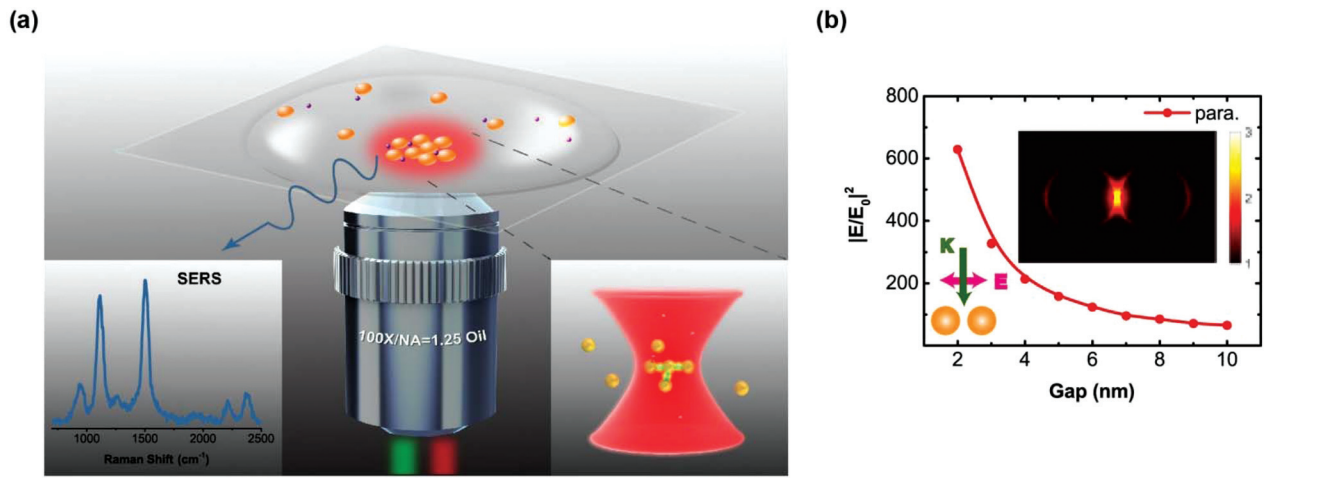

Fig. 1 (a) Schematic illustration of the double-trap system. 1064 nm laser acts as a "macroscopic" trap and 532 nm laser is used to induce interparticle interactions as well as for SERS excitation. Samples are gold colloidal solution including CV molecules. Gold particles are spherical with an average diameter (D) of 20 nm. The inset is a typical SERS spectrum of CV molecules. (b) Calculated electric field enhancement-factor for a gold dimer (D = 20 nm) system in the parallel polarization configuration as a function of interparticle separation d. Calculations have been performed for the position located 0.5 nm from the surface of one of the spheres and at λ = 532 nm. The inset depicts the electric field intensity distributions in the gold dimer with gap size d = 2 nm.

as most metallic nanoaggregates would be pushed away by the strong scattering force as compared to the gradient trapping force.[32] In our experiment, we find that once the 1064 nm laser is switched on, a stable optical trap can be achieved simultaneously (ESI, Movie S1† and Fig. 3b and c). Notably, the trapped particles are gold nanoaggregates instead of isolated particles, as the particles successively approach the trap region within 10 s (see ESI, Movie S1†). Previously, these trapped particles repel each other due to interparticle electrostatic repulsion force, which can be overcome by adding chemical aggregating agents[15,20] to induce aggregation. Here in our pure water solution, we introduce the second green laser to encourage such interparticle attraction forces. As shown in Fig. 1b, such a green laser coincides with the localized surface plasmon resonance of GNPs to induce nano-meter size hot spots. Consequently, these optical hot spots create strong gradient forces to bond these particles,[28] further reducing their gap spacing controlled by the second trap laser.

Here, nanogaps in these nanoaggregates play a crucial role in SERS applications as studied in the solid-state platform such as nanoholes and nanowires.[33–35] In most cases, the gap spacing inversely scales the magnitude of the local EM field, which determines SERS enhancement.[9–11] But how to control such nanogaps remains a big challenge. Previously, SERS applications required highly demanding nano-fabrications on the solid-state platform[13] or chemically aggregating agents in solution.[19] Here our method opens up a new convenient route to optically control interparticle spacing for SERS enhancement by introducing attraction forces from the second laser. As a result, SERS enhancement takes place at the junctions of the particles, as shown in Fig. 1a, and a SERS spectrum from crystal violet (CV) molecules is shown using green laser excitation with single molecule capability (see Fig. 5). On the other hand, such SERS signals provide us with a new spectroscopic tool to characterize the interparticle gap, given the inverse relationship between the gap and SERS enhancement factor. Examples of examining enhanced fluorescence[36] and plasmonic resonance shifts[15,19] to evaluate gap spacing can be found in the literature. By directly reading out SERS signals, ours provides a new powerful method to estimate nanoaggregates' statistical average gap on the sub-wavelength scale below the microscopic diffraction limit.

2.2 Optical forces in plasmonic gold nanoparticle dimers

The optically induced interparticle interactions between metallic particles can be numerically studied. For two nearby particles, Fig. 2 shows the optical forces experienced by one of the particles as a function of gap size (d) between them. In the case of the parallel polarization incident field (Fig. 2a), the force is attractive for all interparticle separations and increases

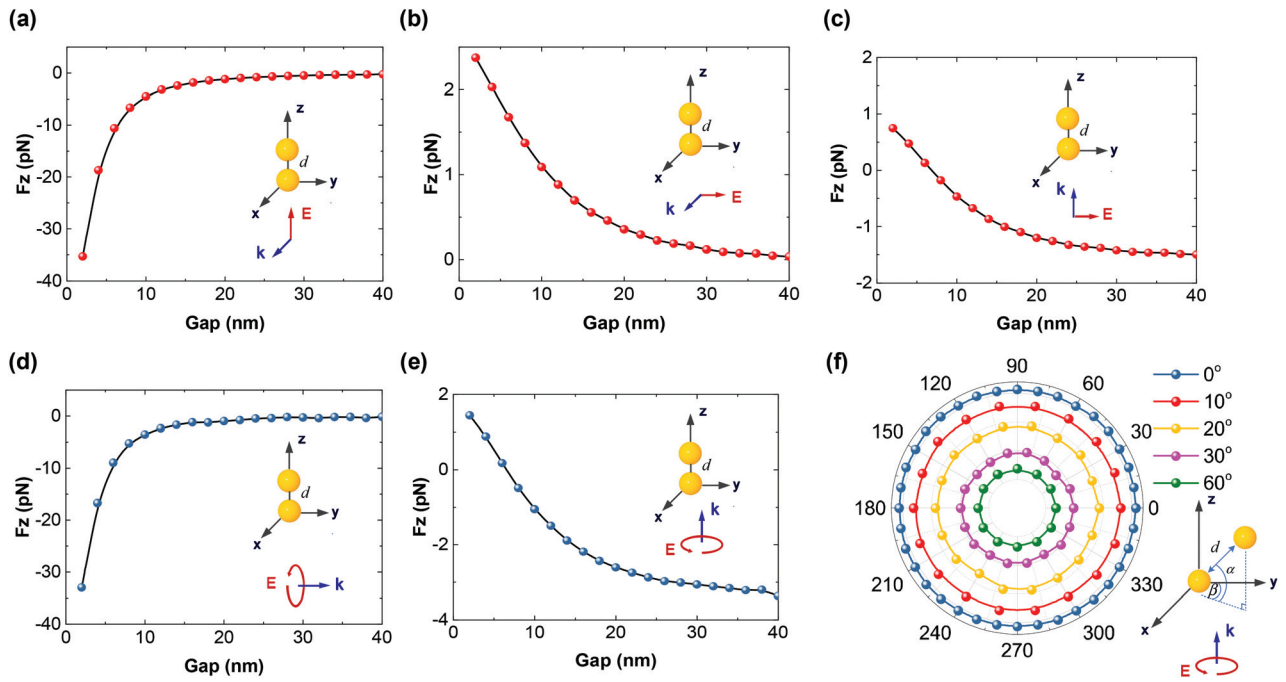

Fig. 2 (a–e) Calculated FZ component of the total optical force between two D = 20 nm GNPs as a function of gap distance d at λ = 532 nm. The insets depict the schematic illustration of configurations for the two-particle (dimer) system in the presence of a plane wave. The wave-vector of the incident wave is denoted by k and its polarization by E. Intensity: 1 W μm^{-2}. The polarization of the incident field is either parallel (a) or perpendicular (b, c) to the dimer axis. (d) and (e) correspond to circularly polarized light incident normal to the dimer surface and along the dimer surface, respectively. (f) Calculated optical forces between two D = 20 nm GNPs λ = 532 nm as a function of the rotation angle (β) of the dimer axis with respect to the y axis at which the angles (α) between the dimer axis and polarization plane (x–y plane) of the incident field are 0°, 10°, 20°, 30° and 60°, respectively. The separation distance is fixed (d = 6 nm). The inset depicts the schematic illustration of configurations for the simulations. The surrounding medium is assumed to be water with refractive index n = 1.33.

dramatically in the spacing range of 2–10 nm. This is a direct consequence of the increasing field-enhancement between the particles due to localized plasmon resonance.[28] As a comparison, the perpendicular polarization case (Fig. 2b) exhibits a repulsive force in the similar range, while the optical force for the end-fire configuration (Fig. 2c) is repulsive for small separations and attractive for larger spacing. These results are consistent with previous reports.[24,37] These different behaviors can be understood from the distribution of induced charges, as discussed in ref. 36. Moreover, the magnitude of the optical attractive force in the parallel configuration is ten times larger than that in the other two cases. Consequently, optical attractive forces in the parallel case for a given linear polarized laser should dominate during nanoaggregate formation, also suggesting that the particles should form lines along the polarization direction[18] and possible near-field manipulation of particles with laser's power and polarization states. As such, we assume that with a circularly polarized incident field, there should be a net aggregation in both directions, as shown in Fig. 2f, where the optical force is symmetrical on the circular polarization plane (x–y plane) when we keep the gap distance constant (d = 6 nm) and rotate one of the particles around the z-axis, and the angles (α) between the dimer axis and polarization plane (x–y plane) of the incident field are 0°, 10°, 20°, 30° and 60°, respectively. It can be seen that the optical forces decrease as α increases and can be safely ignored when $\alpha > 30°$. Therefore, the particles near the plane of polarization may be attracted by interparticle forces and form nano-gaps. Accordingly, a quasi-two-dimensional nanoparticle assembly near the polarization plane can be formed when a circularly polarized field is employed.

As illustrated above, the optical field generates an attractive interparticle force that brings particles within the range of near-field coupling. Previously, the fundamental assumption made by Derjaguin, Landau, Verwey, and Overbeek (DLVO)[20] suggested that the interparticle interaction in a colloid is dominated by additive forces due to screened electrostatic repulsion and van der Waals attraction, respectively. Therefore, the average distance between the particles at a given temperature is determined by three interaction terms: the Coulomb repulsion due to charges at and around the particles, the attractive van der Waals interaction due to spontaneous dipole oscillations, and the optical interparticle force due to coupling between multipolar plasmon oscillations induced by the excitation light. Accordingly, to realize the aggregation of gold particles, the optical forces have to compete with the additive forces considered by DLVO. To be more intuitive, the optical forces are converted into potential energy to compare with DLVO potential. Generally, the DLVO potential works as a repulsive interaction when the interparticle distances are within a few nanometers, and decreases exponentially within the order of tens of nanometers, as illustrated in Fig. S1a.† Meanwhile, the representative optical potential for the same dimer (Fig. S1b†) works as an attractive interaction when the interparticle distance is below 10 nm and this potential is comparable to the DLVO potential. Consequently, we expect that when the laser-induced attractive interparticle interaction is added to the DLVO potential, a potential well should be formed at small separations (below 10 nm) and could be manipulated with laser power without adding any chemical agents.

2.3 SERS in nanoaggregates for gap characterization

In order to investigate the interparticle interactions discussed above, we examine the SERS intensity variation with respect to laser controlled nanoaggregates' characteristics. The GNPs in the experiments are commercially available with mean diameter 20 nm and SPR at ~526 nm. For SERS measurements, samples are prepared by combining 1 mL gold particle solution (with concentrations 10^{-9} M) with 100 μJ aqueous CV solution (10^{-2}–10^{-7} M), which are known to be highly SERS-active.[38] SERS measurements are performed in a home-built microscope setup (100×, NA = 1.25) with the double trap configuration combining 532 nm and 1064 nm lasers. Here the 532 nm laser is loosely focused to avoid possible photothermal damage. A lens (f = 60 mm) is used to separate the focal plane of 532 nm laser and 1064 nm laser, thereby the 532 nm laser is loosely focused on the trapping spot (see Fig. S9 in the ESI†). The power of the incident laser at the sample is 300 mW but the beam waist is adjusted to be of the order of 5 μm in diameter, giving the actual laser intensity 1.5 × 10^6 W cm^{-2}, at which the photo-thermal effect is not very significant during the experiments. The scattered light is passed through a notch filter, resolved by a single-grating spectrometer and detected with a charge-coupled-device (CCD) camera. More details of the experimental setup are given in the ESI.† Firstly, we observed five Raman bands at approximately 724, 868, 1147, 1361, and 1621 cm^{-1} with sole 532 nm excitation in the absence of GNPs in Fig. S2,† all of which are consistent with the previous reports.[38,39] Note that the Raman intensity of pure CV molecules is dependent on CV concentration and not detectable at concentrations lower than 10^{-5} M.

Without the macroscopic trap (1064 nm), Fig. 3a shows a collection of representative SERS spectra acquired from 10^{-5} M CV concentration including gold particles induced by the sole 532 nm laser. The integration time is adjusted to 1 s. Here the SERS intensity from CV has been greatly enhanced compared to that in Fig. S2,† suggesting that GNPs are responsible for the large SERS enhancement. Fig. 3c shows the excitation intensity-dependence of the peak heights of the 1147 cm^{-1} line in different concentrations. Here, the incident power ranges from 5 to 200 mW for 10^{-5} M CV, whereas 2–30 mW for 10^{-3} M and 10^{-4} M CV because the signal is irreversibly lost for high concentrations with incident power above 30 mW. Similar phenomena have been reported.[40–43] However, the physical mechanism of the irreversible quenching of SERS still needs further investigation. A linear dependence of the SERS signal on laser power can be observed justifying the third order nonlinear nature of the Raman process[44] and such a slope varies with CV concentrations, which is a typical response for SERS without interparticle EM coupling or localized gap plasmon resonance.[45] This is because no aggregates

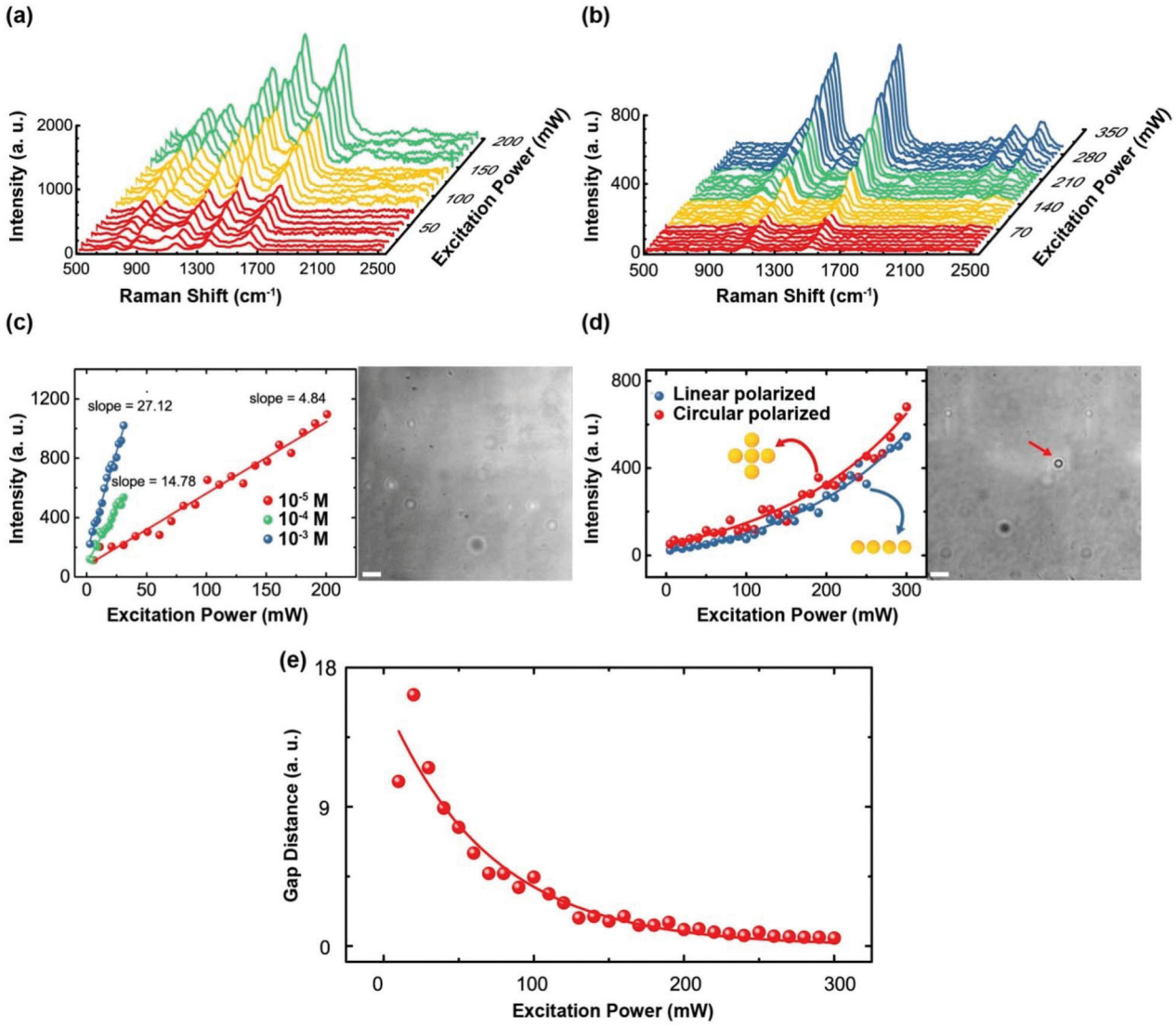

Fig. 3 (a, b) Representatively measured Raman spectra from 10^{-5} M (a) and 10^{-6} M (b) CV solution including GNPs with an increasing power intensity of 532 nm laser with (b) and without (a) the macroscopic trap (1064 nm). Integration time ~1 s. (c) Left: Peak heights of the 1147 cm^{-1} line for the Raman spectra as a function of excitation power at λ = 532 nm only, measured from 10^{-3} M (blue), 10^{-4} M (green) and 10^{-5} M (red) CV solution including GNPs, respectively. The solid lines are the linear fits. Right: CCD images of gold colloids in the probed plane. (d) Left: Peak heights of the 1110 cm^{-1} line for the SERS spectra as a function of excitation power at polarized (blue) and circularly polarized (red) 532 nm excitation with a 1064 nm macroscopic trap, measured from 10^{-6} M CV solution including GNPs. The solid lines are the fits with an exponential function. Right: CCD images of accumulated gold colloids in the trap (red arrow). The scale bar is 3 μm. (e) Gap distance as a function of excitation power using the model $d \propto b{\cdot}D/((I^{SERS}/P)^{1/4} - 1)$, where b is a fitting constant, and I^{SERS} is the SERS intensity in the blue data point of Fig. 3d.

are formed in the laser spot, as seen from the CCD image in Fig. 3c, indicating that the particles are still far apart. In this case, the SERS signal separations (below 10 nm) and the density of nanoaggregates significantly reduce and becomes almost undetectable below a concentration of 10^{-6} M (Fig. S7, details in the ESI†).

As soon as we turn on the 1064 nm laser trap, GNPs gather in the center of the focal spot and form nanoaggregates (Fig. 3d), and simultaneously, the 532 nm laser is also launched to encourage the interparticle forces and excite SERS. As a result, SERS signals can be greatly enhanced and become detectable at 10^{-6} M concentration (Fig. 3b and d), and one major contribution arises from a large number of hot spots inside nanoaggregates.[14,17] However, a nonlinear dependence of the SERS signal on laser power is observed in contrast to the former case (sole trap) where the linear power dependence originates from the one third order of nonlinear response of the fixed structure in nanoparticle solution. This nonlinear power dependence indicates that the optically induced interparticle forces play a crucial role in shrinking gap sizes in these hot spots such that SERS gains a nonlinear enhancement. This phenomenon can be qualitatively explained as follows: imagine a row of particles of diameter D (20 nm) separated by gaps of length d arranged parallel to a

uniform electrostatic field E_0. If we make the crude approximation that the particles are perfectly conducting, the local field in the gap can be approximated by $E_{loc} \approx E_0(D + d)/d$.[46] The SERS enhancement factor, commonly approximated as the fourth power of the field enhancement in the local optical fields of the metal particles,[46] is then given by $M \approx (D/d + 1)^4$, where M is the enhancement factor. Accordingly, the SERS intensity can be expressed by the following equation: $I^{SERS} \propto b{\cdot}P{\cdot}(D/d + 1)^4$, where P is the incident power and b is a fitting constant. Note that such enhancement is pronounced when $d < D$. This can also be verified by a numerical study of electric field enhancement $|E_{loc}/E_0|^2$ as shown in Fig. S4,† where the simple electrostatic "voltage division" model $(D/d + 1)^2$ is in excellent agreement with the simulation results, similar to the previous approach.[26] Consequently, from the above formulism, we derive a gap variation with respect to the excitation power as shown in Fig. 3e from the measured SERS signals. The results in Fig. 3e qualitatively provide the deduction trend of gap with increasing trapping laser power. To be clear, the gap distance in the ordinate is dimensionless because the fitting constant (b) in the model $d \propto b{\cdot}D/((I^{SERS}/P) - 1)$ is not certain.

Moreover, two peaks centered at 2217 cm^{-1} and 2378 cm^{-1} are detected unexpectedly in Fig. 3b, which have never been reported in the literature. This can be attributed to the inter-particle coupling in nanoaggregates that selectively enhances the two Raman bands. Finally, we observe that the trapped nanoaggregates fall apart and float away once the trapping laser is turned off, which indicates that such nanoaggregates are not permanently bonded and the gap spacing is reversibly controlled by optical forces. Therefore, this optically tunable method is more useful compared with the previous methods of adding chemically aggregating agents because the chemicals could easily cause permanent aggregation and hinder reutilization of particles. In addition, previous work has found that the SERS intensity decreased below a gap size of around 5.5 nm due to a lower EM coupling efficiency.[47] While we haven't observed any degradation of SERS when increasing the laser power in our case, the balance of inter-molecule forces and induced optical ones prevents such situation.

The polarization state of trapping laser is also crucial in our experiments. In Fig. 3d, the SERS intensity is slightly stronger under the incident circularly polarized field compared with the linear polarized ones, especially for high incident powers. For the linear incident laser, the particles prefer to form a series of line-shape nanoaggregates along the polarization direction,[48] while the circular polarization creates an effective two-dimensional possibility for inter-particle trapping. Previous work[49] suggests that the micro-structure of nanoparticle aggregates can affect the polarization state of Raman scattering. Here we investigate SERS polarization states from these trapped nanoaggregates as an indirect probe to study their microscopic arrangement. The polarization relationship between the Raman spectrum and 1064 nm laser is demonstrated in Fig. S6(a and b).† The results show that the total intensity of the scattered light is always maximized along the direction o532 nm polarization. Thus, the polarization of the 1064 nm laser can hardly influence the Raman results. Furthermore, Fig. S6(c)† provides theoretical analysis of this phenomenon. As can be seen, the magnitude of the optical force is much smaller at λ = 1064 nm than at the dimer resonance (λ = 532 nm) and can be safely neglected. As a result, the polarization of the 1064 nm laser does not affect the results of the Raman spectrum. Afterwards, we demonstrated the polarization relationship between the Raman spectrum and 532 nm laser in Fig. 4. For the linear polarized case in Fig. 4a and b, the total intensity of the scattered light is maximized along the direction of the incident polarization, indicating that the particles may roughly form lines along the polarization direction during aggregation, due to the strong attraction force induced by the linear polarized laser as shown in Fig. 3. The morphology of the aggregates probably cannot align in an absolutely straight line due to the Brownian movement.[15] Therefore it is possible that the SERS intensity is a bit tilted with respect to the polarization as can be seen in Fig. 4b. On the other hand, for the circularly polarized case in Fig. 4c, the SERS polarization profile exhibits a random manner without a preferred axis as the former one, which is an outcome of the two-dimensional axial symmetry of the nanoaggregates' struc-

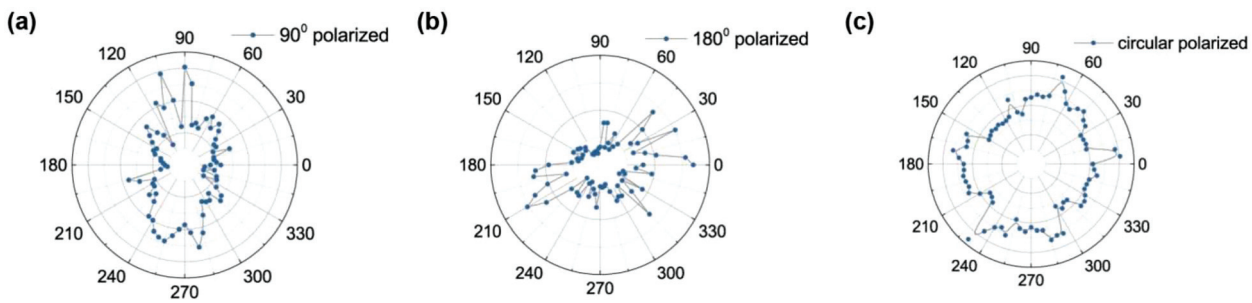

Fig. 4 SERS intensity corresponding to the peak band (1110 cm^{-1}) of CV molecules (10^{-6} M) at the trapping spot as a function of the angle of rotation of Raman polarization, obtained with 90° polarized (a), 180° polarized (b) and circularly polarized (c) 532 nm excitation, respectively. Laser power ~2.5 × 10^5 W cm^{-2}. Integration time ~1 s. Since the response of a nanoparticle aggregate can be probed through the process of Raman scattering (RS) from molecules residing within the aggregate, we evaluate the profiles of RS intensity corresponding to the peak band (1110 cm^{-1}) of CV molecules (10^{-6} M) at the trapping spot obtained with 90° polarized, 180° polarized and circularly polarized 532 nm excitation respectively (see Fig. 5).

ture induced by the circularly polarized laser. This observed polarization dependence provides key evidence that the micro-arrangement of nanoaggregates is indeed responsible for the SERS polarization states, and we do not observe similar behavior of SERS without the optical trap despite incident laser's polarization. Such manipulation through the polarization state provides us with another important route to control these nanoaggregates on the micro-scale below the diffraction limit.

2.4 SERS at single-molecule limit

Fig. 5 shows SERS sensing applications with single molecule sensitivity by implementing the above double trap scheme. In order to claim SM-SERS, we employ the bi-analyte SM-SERS method developed by Etchegoin and Ru.[50,51] This technique is based on spectroscopic contrast between two different kinds of SERS-active molecules, and importantly, does not rely on the ratio of the number of molecules to the nanoparticles used in the experiments. The two molecules used for our experiments are Nile Blue (NB) and Crystal Violet (CV) at 10^{-7} M concentration. For SM-SERS experiments, we choose 1645 and 1110 cm^{-1} Raman modes of NB and CV, respectively. Fig. 5a shows the time evolution of the bi-analyte SM-SERS signal captured from the trap of gold nanoparticles. The total number of spectra collected is 850, and the acquisition time for each spectrum is 1 s and the dwell time between consecutive accumulations is 1 s. The average spectra of solutions NB and CV show distinguishable SERS spectra. Because of the large number of molecules, the SERS signal should in principle always be a mixture of these two dyes. The observation of a SERS signal of purely one type of dye is clear evidence that it comes from a very small number of molecules. Thus, our method not only creates multiple plasmonic hot spots in a nanoparticle assembly but also probes the single molecule spectral signatures simultaneously. Note that for a 10^{-7} M concentration molecule solution, SERS signals exhibit a random time-fluctuating fashion. In our case, these hot spots are highly localized in the range of 10 nm (see Fig. 1), for CV molecules with low concentrations, and molecules randomly pass these active region due to the Brownian movement, resulting in a statistical temporal fluctuation. Such behavior is only pronounced in a few-molecule limit, but average out with increasing concentrations.

In our experiment, the actual volume size of nanoaggregates is hard to access because it is below the diffraction limit. We estimate that around 30 particles are trapped, giving $\sim 2.16 \times 10^{-4}$ μm^3 volume. The number of trapped particles is estimated through single particle counting[36] according to the video recording (see Movie S1 in the ESI†). For a more realistic estimation, the SERS sensing area can be approximated by the focal spot size of trap laser 0.67 μm × 0.67 μm × 1.36 μm = 0.6 μm^3, and this contains less than 1 molecule for a 10^{-8} M concentration CV solution. Even for such low concentration, our method is still capable of detecting SERS as shown in Fig. 6, where similar temporal fluctuations are also observed. Hence, our double trap method can provide a sensitive scheme for SERS sensing at a low molecule level. In the future, we expect that microfluidics platforms, where it is hard to fabricate SERS active structures,[52] may be integrated with our fabrication-free double laser trap scheme in order to achieve single molecule SERS sensing application.

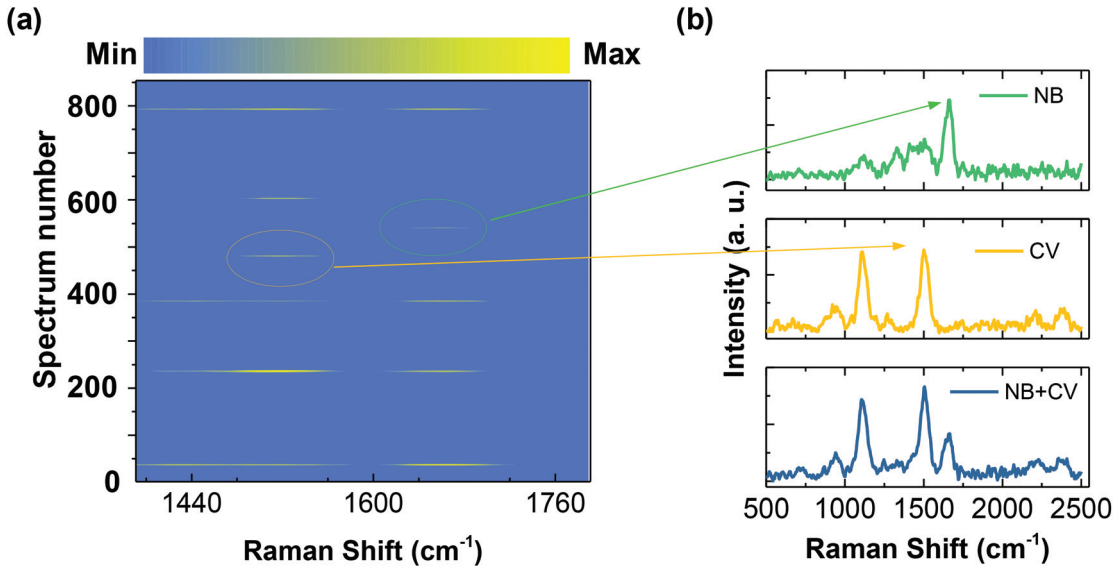

Fig. 5 Single-molecule SERS from the aggregated gold nanoparticles. (a) Bi-Analyte (Nile Blue (NB) and Crystal Violet (CV)) SERS time-series spectra recorded from the trap of gold nanoparticles. The concentration of both the molecules is 10^{-7} M. For analysis, 1645 cm^{-1} mode of NB and 1110 cm^{-1} mode of CV are considered. 850 spectra have been displayed to show spectral fluctuation of single molecules. Signal acquisition time is 1 s. All the data are collected using 532 nm excitation wavelength (20 mW power before entering the objective). (b) Representative individual spectra showing a pure NB event, a pure CV event, and a mixed event.

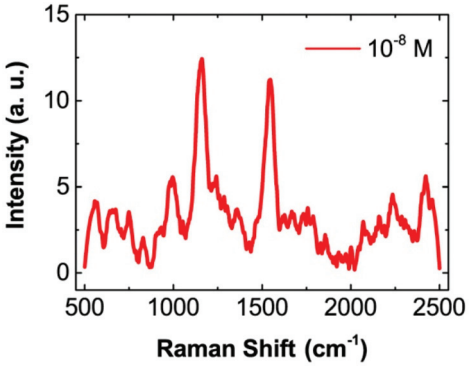

Fig. 6 SERS spectra of 10^{-8} M CV. Laser power ~2.5 × 10^5 W cm^{-2}. Integration time ~10 s.

3. Conclusions

In summary, we have proposed a double trap method of optically induced aggregation of GNPs. This method has been used to create SERS active hot spots without adding any chemical or functionalization. On these sites, the Raman spectrum of CV molecules has been remarkably enhanced by the optical force induced aggregation process, which can further provide a sensitive scheme for SERS sensing at a single molecule level. The optical interaction forces between particle dimers are theoretically investigated by using the finite-difference time-domain (FDTD) technique combined with the Maxwell stress tensor formalism. We show that a substantial plasmon enhanced attractive force at short gap spacing occurs in the parallel polarization configuration. The result is also corroborated by SERS experiments on optically aggregated gold colloids, which shows that we extend optical aggregation into the Rayleigh regime by employing optical forces. Additionally, by directly reading out SERS signals, our method paves a new powerful way for estimating nanoaggregates' statistical average gap on the sub-wavelength scale below the microscopic diffraction limit. These results could significantly influence surface-enhanced Raman scattering and related spectroscopy techniques under normal experimental conditions and contribute to single-molecule sensitivity as demonstrated by our experiments.

Conflicts of interest

There are no conflicts to declare.

Acknowledgements

This work was supported by the National Key Research and Development program (Grant No. 2016YFA0302500), the National Science Foundation of China (Grant No. 11674228, No. 11304201, No. 61475100), the National 1000-plan Program (Youth), the Shanghai Scientific Innovation Program (Grant No. 14JC1402900), and the Shanghai Scientific Innovation Program for International Collaboration (Grant No. 15220721400).

Notes and references

1 K. Kneipp, Y. Wang, H. Kneipp, L. T. Perelman, I. Itzkan, R. R. Dasari and M. S. Feld, *Phys. Rev. Lett.*, 1997, **78**, 1667.
2 S. Nie and S. R. Emory, *Science*, 1997, **275**, 1102–1106.
3 Y.-w. Jun, S. Sheikholeslami, D. R. Hostetter, C. Tajon, C. S. Craik and A. P. Alivisatos, *Proc. Natl. Acad. Sci. U. S. A.*, 2009, **106**, 17735–17740.
4 S. Chen, M. Svedendahl, R. P. Van Duyne and M. Käll, *Nano Lett.*, 2011, **11**, 1826–1830.
5 D. Huang, C. P. Byers, L.-Y. Wang, A. Hoggard, B. Hoener, S. Dominguez-Medina, S. Chen, W.-S. Chang, C. F. Landes and S. Link, *ACS Nano*, 2015, **9**, 7072–7079.
6 D. Sivun, C. Vidal, B. Munkhbat, N. Arnold, T. A. Klar and C. Hrelescu, *Nano Lett.*, 2016, **16**, 7203–7209.
7 A. Slablab, L. Le Xuan, M. Zielinski, Y. de Wilde, V. Jacques, D. Chauvat and J.-F. Roch, *Opt. Express*, 2012, **20**, 220–227.
8 M. Celebrano, X. Wu, M. Baselli, S. Großmann, P. Biagioni, A. Locatelli, C. De Angelis, G. Cerullo, R. Osellame and B. Hecht, *Nat. Nanotechnol.*, 2015, **10**, 412.
9 J. A. Schuller, E. S. Barnard, W. Cai, Y. C. Jun, J. S. White and M. L. Brongersma, *Nat. Mater.*, 2010, **9**, 193.
10 H. Duan, A. I. Fernández-Domínguez, M. Bosman, S. A. Maier and J. K. Yang, *Nano Lett.*, 2012, **12**, 1683–1689.
11 D. Marinica, A. Kazansky, P. Nordlander, J. Aizpurua and A. G. Borisov, *Nano Lett.*, 2012, **12**, 1333–1339.
12 W. Zhu, R. Esteban, A. G. Borisov, J. J. Baumberg, P. Nordlander, H. J. Lezec, J. Aizpurua and K. B. Crozier, *Nat. Commun.*, 2016, **7**, 11495.
13 L. Gunnarsson, E. Bjerneld, H. Xu, S. Petronis, B. Kasemo and M. Käll, *Appl. Phys. Lett.*, 2001, **78**, 802–804.
14 L. Polavarapu and Q.-H. Xu, *Langmuir*, 2008, **24**, 10608–10611.
15 H. Eckstein and U. Kreibig, *Z. Phys. D*, 1993, **26**, 239–241.
16 K. Murakoshi and Y. Nakato, *Adv. Mater.*, 2000, **12**, 791–795.
17 Y. Tanaka, H. Yoshikawa, T. Itoh and M. Ishikawa, *J. Phys. Chem. C*, 2009, **113**, 11856–11860.
18 Y. Tanaka, H. Yoshikawa, T. Itoh and M. Ishikawa, *Opt. Express*, 2009, **17**, 18760–18767.
19 L. Tong, V. D. Miljkovic, P. Johansson and M. Kall, *Nano Lett.*, 2010, **11**, 4505–4508.
20 G. M. Kontogeorgis and S. Kiil, *Introduction to applied colloid and surface chemistry*, John Wiley & Sons, 2016.
21 A. Ashkin, J. M. Dziedzic, J. Bjorkholm and S. Chu, *Opt. Lett.*, 1986, **11**, 288–290.
22 J. Prikulis, F. Svedberg, M. Käll, J. Enger, K. Ramser, M. Goksör and D. Hanstorp, *Nano Lett.*, 2004, **4**, 115–118.
23 P. M. Hansen, V. K. Bhatia, N. Harrit and L. Oddershede, *Nano Lett.*, 2005, **5**, 1937–1942.

24 A. Hallock, P. Redmond and L. Brus, *Proc. Natl. Acad. Sci. U. S. A.*, 2005, **102**, 1280–1284.
25 P. Chu and D. Mills, *Phys. Rev. Lett.*, 2007, **99**, 127401.
26 T. U. Tumkur, X. Yang, B. Cerjan, N. J. Halas, P. Nordlander and I. Thomann, *Nano Lett.*, 2016, **16**, 7942–7949.
27 Z. Yan, R. A. Shah, G. Chado, S. K. Gray, M. Pelton and N. F. Scherer, *ACS Nano*, 2013, **7**, 1790–1802.
28 H. Xu and M. Käll, *Phys. Rev. Lett.*, 2002, **89**, 246802.
29 A. S. Zelenina, Q. Romain and N. V. Manuel, *Opt. Lett.*, 2007, **32**, 1156–1158.
30 Z. Li, M. Käll and H. Xu, *Phys. Rev. B: Condens. Matter Mater. Phys.*, 2008, **77**, 439–446.
31 L. Tong, M. Righini, M. U. Gonzalez, R. Quidant and M. Käll, *Lab Chip*, 2009, **9**, 193–195.
32 K. Toussaint, M. Liu, M. Pelton, J. Pesic, M. Guffey, P. Guyot-Sionnest and N. Scherer, *Opt. Express*, 2007, **15**, 12017–12029.
33 A. G. Brolo, E. Arctander, R. Gordon, B. Leathem and K. L. Kavanagh, *Nano Lett.*, 2004, **4**, 2015–2018.
34 P. P. Patra, R. Chikkaraddy, R. P. Tripathi, A. Dasgupta and G. P. Kumar, *Nat. Commun.*, 2014, **5**, 4357.
35 H. Wei, F. Hao, Y. Huang, W. Wang, P. Nordlander and H. Xu, *Nano Lett.*, 2008, **8**, 2497–2502.
36 C. Hosokawa, H. Yoshikawa and H. Masuhara, *Phys. Rev. E: Stat., Nonlinear, Soft Matter Phys.*, 2005, **72**, 021408.
37 V. D. Miljkovic, T. Pakizeh, B. Sepulveda, P. Johansson and M. Kall, *J. Phys. Chem. C*, 2010, **114**, 7472–7479.
38 E. Liang, X. Ye and W. Kiefer, *J. Phys. Chem. A*, 1997, **101**, 7330–7335.
39 S. L. Kleinman, E. Ringe, N. Valley, K. L. Wustholz, E. Phillips, K. A. Scheidt, G. C. Schatz and R. P. Van Duyne, *J. Am. Chem. Soc.*, 2011, **133**, 4115–4122.
40 Y. Sharaabi, T. Shegai and G. Haran, *Chem. Phys.*, 2005, **318**, 44–49.
41 Y.-S. Choi, J.-J. Kim and S. Miyajima, *Chem. Phys. Lett.*, 1996, **255**, 45–48.
42 S. H. Macomber and T. E. Furtak, *Solid State Commun.*, 1983, **45**, 267.
43 A. Otto, J. Billmann, J. Eickmans, U. Ertürk and C. Pettenkofer, *Surf. Sci.*, 1984, **138**, 319–338.
44 R. W. Boyd, *Nonlinear optics*, Elsevier, 2003.
45 A. R. Salmon, R. Esteban, R. W. Taylor, J. T. Hugall, C. A. Smith, G. Whyte, O. A. Scherman, J. Aizpurua, C. Abell and J. J. Baumberg, *Small*, 2016, **12**, 1788–1796.
46 H. Xu, E. J. Bjerneld, J. Aizpurua, P. Apell, L. Gunnarsson, S. Petronis, B. Kasemo, C. Larsson, F. Hook and M. Kall, *Interparticle coupling effects in surface-enhanced Raman scattering*, 2001.
47 Y. Yokota, K. Ueno and H. Misawa, *Chem. Commun.*, 2011, **47**, 3505–3507.
48 C. Park and R. E. Robertson, *Mater. Sci. Eng., A*, 1998, **257**, 295–311.
49 T. Shegai, Z. Li, T. Dadosh, Z. Zhang, H. Xu and G. Haran, *Proc. Natl. Acad. Sci. U. S. A.*, 2008, **105**, 16448–16453.
50 E. C. Le Ru, M. Meyer and P. G. Etchegoin, *J. Phys. Chem. B*, 2006, **110**, 1944–1948.
51 P. G. Etchegoin, M. Meyer, E. Blackie and E. C. Le Ru, *Anal. Chem.*, 2007, **79**, 8411–8415.
52 K. R. Strehle, D. Cialla, P. Rösch, T. Henkel, M. Köhler and J. Popp, *Anal. Chem.*, 2007, **79**, 1542–1547.